

RESEARCH

Open Access



# Gene signatures, immune infiltration, and drug sensitivity based on a comprehensive analysis of m<sup>6</sup>A RNA methylation regulators in cervical cancer

Xiaoqin Lu, Rui Li, Yanqi Ying, Wenyi Zhang and Wuliang Wang\* 

## Abstract

**Background:** Cervical cancer is the fourth most common cancer in women. N<sup>6</sup>-dimethyladenosine (m<sup>6</sup>A) mRNA methylation is closely associated with cervical cancer.

**Methods:** Using TCGA database, we studied the expression and mutation of m<sup>6</sup>A-related genes in cervical squamous cell carcinoma and endocervical adenocarcinoma (CESC) and obtained genetic characteristics based on an m<sup>6</sup>A risk model and prognostic value of m<sup>6</sup>A. We studied the effects of the m<sup>6</sup>A risk score on immune features and genomic changes of patients with CESC, evaluated the sensitivity of patients with CESC to different small-molecule drugs based on the m<sup>6</sup>A risk score, and established a clinical prediction model.

**Results:** Ten m<sup>6</sup>A-related genes were differentially expressed between CESC and normal tissues. High-risk patients had a low overall survival (OS) and significantly low immune scores but showed no significantly altered stromal scores. The tumor mutation burden (TMB) and tumor neoantigen levels significantly differed between the high- and low-risk groups. In the high-risk group, copy number variation (CNV) changes mainly led to gene amplification, while in the low-risk group, CNV changes primarily manifested as gene copy number deletions. ZC3H13 expression was low in CESC tissues. ZC3H13 knockdown promoted CESC cell proliferation, migration, and invasion, reducing the RNA methylation levels. Rapamycin suppressed the CESC cell proliferation, migration, and invasion abilities, increasing the m<sup>6</sup>A levels.

**Conclusion:** m<sup>6</sup>A mRNA methylation is closely related to the occurrence, development, immune invasion, drug sensitivity, and prognosis of cervical cancer. The prognostic m<sup>6</sup>A feature model of m<sup>6</sup>A signature genes can accurately predict the OS of patients with CESC. Drugs targeting factors regulating m<sup>6</sup>A mRNA methylation might offer a good prospect for treating cervical cancer.

**Keywords:** N<sup>6</sup>-dimethyladenosine, Immune infiltration, Drug sensitivity, Cervical cancer, ZC3H13, Rapamycin

## Introduction

Cervical cancer is the fourth most common cancer in women [1, 2]. More than 570,000 new cases of cervical cancer are diagnosed worldwide each year, with approximately 311,000 deaths [3]. Presently, at least 170 RNA modifications have been discovered in cervical cancer, for instance, N<sup>6</sup>-dimethyladenosine (m<sup>6</sup>A), inosine,

\*Correspondence: wangwuliang@zzu.edu.cn

Department of Obstetrics and Gynecology, the Second Affiliated Hospital of Zhengzhou University, 2nd, Jingba Road Henan Province, Zhengzhou 450053, China



© The Author(s) 2022. **Open Access** This article is licensed under a Creative Commons Attribution 4.0 International License, which permits use, sharing, adaptation, distribution and reproduction in any medium or format, as long as you give appropriate credit to the original author(s) and the source, provide a link to the Creative Commons licence, and indicate if changes were made. The images or other third party material in this article are included in the article's Creative Commons licence, unless indicated otherwise in a credit line to the material. If material is not included in the article's Creative Commons licence and your intended use is not permitted by statutory regulation or exceeds the permitted use, you will need to obtain permission directly from the copyright holder. To view a copy of this licence, visit <http://creativecommons.org/licenses/by/4.0/>. The Creative Commons Public Domain Dedication waiver (<http://creativecommons.org/publicdomain/zero/1.0/>) applies to the data made available in this article, unless otherwise stated in a credit line to the data.

pseudouridine, 5-methylcytidine (m5C), 5-hydroxymethylcytidine (hm5C), and N1-methyladenosine (m1A). Furthermore, most RNA species contain at least one chemical modification and are widely associated with physiopathological processes [4–7]. m<sup>6</sup>A is one of the most abundant mRNA modifications [8, 9]. m<sup>6</sup>A modifies approximately 0.1–0.4% of all adenosines in RNA, accounting for ~50% of the total methylated ribonucleotides [10]. m<sup>6</sup>A is a dynamic and reversible epigenetic modification. The cellular m<sup>6</sup>A status is regulated by groups of proteins called m<sup>6</sup>A methyltransferases (“writers”), m<sup>6</sup>A demethylases (“erasers”), and m<sup>6</sup>A-binding proteins (“readers”), which add, remove, or recognize m<sup>6</sup>A-modified sites, respectively, modulating the stability, splicing, intracellular distribution, and translational changes of mRNA while affecting certain biological processes [11–14]. As a potential tumor biomarker, m<sup>6</sup>A plays a key role in various biological processes and malignancies [15]. Changes in m<sup>6</sup>A-modifying enzyme levels affect the expression of downstream oncogenes or tumor suppressor genes by altering mRNA methylation [16]. Furthermore, epigenetic markers potentially serve as diagnostic, prognostic, and predictive biomarkers and might be used as novel targets for cancer precision medicine [17–20].

Here, we studied the expression and mutation of m<sup>6</sup>A-related genes in patients with cervical squamous cell carcinoma and endocervical adenocarcinoma (CESC), obtained the gene characteristics of patients with CESC based on an m<sup>6</sup>A-risk model, and constructed a prognostic m<sup>6</sup>A feature model based on m<sup>6</sup>A signature genes. The effects of the m<sup>6</sup>A risk score on biological function, immune characteristics, and genomic changes of patients with CESC were analyzed. The sensitivity of patients with CESC to different small molecule drugs was evaluated based on the m<sup>6</sup>A risk score, and a clinical prediction model was constructed. Subsequently, we studied the expression and function of ZC3H13 in cervical cancer tissues according to the screening results. We selected rapamycin to study the effects of the screened drug on m<sup>6</sup>A and cervical cancer phenotype. Through this research, we attempted to study the gene signatures, immune infiltration, and drug sensitivity based on a comprehensive analysis of m<sup>6</sup>A RNA methylation regulators in cervical cancer.

## Materials and methods

### Data

Data were downloaded from the TCGA GDC website (<https://portal.gdc.cancer.gov/>), and the cervical squamous carcinoma and adenocarcinoma (cervical squamous cell carcinoma and endocervical adenocarcinoma, CESC) expression profile data (FPKM results) of gene expression sequencing in patients were obtained. The

FPKM values were converted into the TPM values as follows:

$$\text{TPM}_i = \left( \frac{\text{FPKM}_i}{\sum_j \text{FPKM}_j} \right) \cdot 10^6$$

Clinical data of corresponding patients, including age, TNM stage, and survival prognosis, were downloaded. After excluding patients with CESC with missing clinical information, data regarding 279 tumor tissues and three paracancer tissues were obtained. The copy number variation (CNV) of somatic cells of patients with CESC was downloaded. RCircos package was used to map the gene CNV in 23 pairs of chromosomes [21]. “Masked mutation” was selected as the somatic mutation data, and R’s MAFTools package was used to visualize somatic mutations. The tumor mutation burden (TMB) of each patient was obtained [22]. The sequencing results of 19 cervical tissues were downloaded from the GTEx database and converted into TPM values.

In addition, gene expression data of the GSE52903 chip, clinicopathological features, and prognostic information of patients were downloaded from samples in the GEO database, including 55 tumor tissue and 17 normal cervical tissue samples [23]. Among them, all chip data samples were from *Homo Sapiens*, and the platform was mainly based on the GPL6244 [Hugene-1\_0-ST] Affymetrix Human Gene 1.0 ST Array [Transcript (Gene) version]. Next, TCGA data, GTEx data, and GEO chip data were combined, and the limma and sva packages of R were used for homogenization and batch removal [24, 25]. The total process is composed of two steps. The first is data consolidation; only common genes and corresponding expression values are retained in the three data sets. The second step involves removing the batch effects. The first step adopts the merge function in R to merge the three data sets. The second step uses the combat function in the SVA package to remove the batches. The demographic and clinical characteristics of the cervical cancer patients are shown in Additional file 1 materials.

### Risk model construction based on m<sup>6</sup>A-related genes

To analyze the expression of m<sup>6</sup>A-related genes in cervical cancer, we first analyzed the differential expression of m<sup>6</sup>A-related genes in cervical cancer and normal tissues, the correlation of gene expression, and its impact on the prognosis of patients with CESC. Subsequently, expression data of patients with CESC were pooled using TCGA-CESC and GEO data. m<sup>6</sup>A-related genes were included in the model, and the least absolute shrinkage and selection operator (LASSO) algorithm was used to analyze the dimension reduction and

obtain characteristic genes associated with prognosis. A risk score formula was established using the penalty coefficient weighted normalized gene expression values obtained by LASSO Cox analysis. The patients were divided into high- and low-risk groups based on the median risk score.

$$\text{riskScore} = \sum_i \text{Coefficient}(\text{hubgene}_i) * \text{mRNAExpression}(\text{hubgene}_i)$$

### Gene set enrichment analysis (GSEA)

Gene Ontology (GO) analysis is a common method for large-scale functional enrichment studies that includes three categories: biological process (BP), molecular function (MF), and cellular component (CC). KEGG is a widely used database that stores information regarding genomes, biological pathways, diseases, and drugs. R's clusterProfiler package was used for GO annotation analysis and KEGG pathway enrichment analysis of signature genes. A value of FDR < 0.05 was considered statistically significant [26].

To study the differences in BPs between different subgroups, we performed GSEA based on the gene expression profile dataset of patients with CESC. GSEA is a computational method to analyze whether a specific gene set has statistically significant differences between two biological states and is usually used to estimate changes in pathways and BP activity among samples [27]. The "h.all.v7.2.symbols.gmt" gene set was downloaded from MSigDB for GSEA analysis [27]. An adjusted P-value of less than 0.05 was considered statistically significant.

### Assessment of patients' biological characteristics between risk groups

We further analyzed the correlation between different subgroups and some biologically related processes using the GSVA method [27]. Mariathan et al. constructed a gene set for storing genes related to some BPs, including (1) immune checkpoint; (2) antigen processing; (3) characteristics of CD8<sup>+</sup> T cells; (4) epithelial-mesenchymal transformation (EMT) markers, including EMT1, EMT2, and EMT3; (5) angiogenesis; (6) characteristics of TGF- $\beta$  response in pan-FTBRs; (7) WNT characteristics; (8) DNA damage repair; (9) mismatch repair; (10) nucleotide excision repair; (11) DNA replication; and (12) antigen handling and presentation [28–30]. Gene sets corresponding to different biological characteristics were downloaded to calculate the corresponding enrichment scores of patients and to compare the differences between two groups.

### Analysis of m<sup>6</sup>A-related differentially expressed genes (DEGs)

To identify genes associated with the m<sup>6</sup>A risk model, THE limma package of R was used to analyze DEGs between high and low subgroups in patients with CESC, and the DEGs with significant differences were defined as

genes with absolute log (Fold change) > 0.5 and FDR < 0.05 [24]. Hierarchical clustering was used to divide the tumors into different gene groups based on the Euclidean distance of differential gene expression and named them Geneclusters A, B, and C. Among them, R's Consensus-ClusterPlus package was used to determine the number of clusters in the dataset and was repeated 1000 times to ensure the stability of classification [31]. Meanwhile, based on the expression changes of specific genes, they were divided into signature-A and -B gene groups.

### Calculation of dimensionality reduction and m<sup>6</sup>A score

First, unsupervised clustering was used to classify TCGA data of patients according to DEG values. m<sup>6</sup>A signature-A and -B gene groups were reduced in dimension according to the Boruta algorithm. The principal component PC1 was extracted by the principal component analysis (PCA) algorithm as the A score. Finally, we applied a method similar to the gene expression grade index to define each patient's immune checkpoint inhibitor (ICI) score:

$$m6Ascore = \sum_i PC1A - \sum_i PC1B$$

### Identification and correlation analysis of tumor immune infiltrating cells

To further quantify the proportion of different immune cells in CESC samples, the CIBERSORT algorithm, and LM22 gene set were used to investigate the phenotypes of 22 human immune cells (including B cells, T cells, and natural killer cells) in the tumor microenvironment (TME) [32]. Macrophages are highly sensitive and specific. CIBERSORT is a deconvolution algorithm that uses a set of reference gene expression values (with 547 characteristic genes) considered to be the minimum representative of each cell type. Based on these values, the proportion of cell types can be inferred in data from a large tumor sample with mixed cell types.

At the same time, R's ESTIMATE package was used to assess tumor immune activity [33]. ESTIMATE an

immune score for each tumor sample obtained by quantifying the immune activity (level of immune invasion) in the tumor sample based on its gene expression profile. Then, differences in the characteristics of immune infiltration in patients with CESC between the high- and low-risk groups were obtained.

#### Analysis of CNV

To analyze the changes in the copy number in different risk score groups of TCGA-patients with CESC, the TCGAbiolinks package of R was used to download the masked copy number segment data of patients. GISTIC 2.0 analysis of the downloaded CNV fragments was performed by GenePattern5. During analysis, except for a few parameters (e.g., the confidence is 0.99; Excluding X chromosomes prior to analysis), GISTIC 2.0 analysis was used with the default settings. Finally, R's MAfTools package was used to visually display the results of the GISTIC 2.0 analysis.

#### Sensitivity analysis of anticancer drugs

Genomics of Drug Sensitivity in Cancer (GDSC; <https://www.cancerrxgene.org/>), which is used for molecular cancer therapy and mutation, was used to explore public databases [34]. R's pRRophetic package was used to download cell line gene mutation data and IC<sub>50</sub> values of different anticancer drugs to analyze the correlation between patients with high- and low-risk scores and sensitivity to different anticancer drugs [35].

#### Building a clinical prediction model based on the m<sup>6</sup>A risk model

To prove that the risk score combined with the clinicopathological features can help in the personalized assessment of patient prognosis, univariate and multivariate Cox analyses were conducted to analyze the ability of the risk score combined with clinicopathological features to predict the overall survival (OS). Then, a nomogram was constructed by incorporating the risk scoring model and clinicopathological features into the model. To quantify the differentiated performance, Harrell's Consistency index (C-index) was measured. A calibration curve was generated to evaluate the performance of the rosette by comparing the predicted values of the rosette with the actual observed survival rates.

#### Human tissue samples

Ten cervical cancer tissues and ten normal cervical tissues were obtained from patients with cervical cancer who underwent ovariectomy prior to chemotherapy and radiotherapy. The resected cervical cancer tissues and normal tissues were immediately stored at -80 °C for further study. All patients signed informed consent

forms. This study was performed in accordance with the Helsinki Declaration and approved by the ethics committee of the Second Affiliated Hospital of Zhengzhou University.

#### Cell lines and culture conditions

The human cervical cancer cell lines HeLa and SiHa were purchased from Procell Life Science & Technology Co., Ltd. (Wuhan, P.R. China). To prepare the complete growth medium, the cell culture media were supplemented with fetal bovine serum (Gibco, Grand Island, USA) at a final concentration of 10%.

#### RNA extraction

Total RNAs of human cells were extracted using the Trizol reagent (Invitrogen, Carlsbad, CA, USA) according to the manufacturer's instructions and treated with RQ1 DNase (Promega, Madison, WI, USA) to remove DNA. The quality and quantity of purified RNA were determined by measuring the absorbance at 260 nm and 280 nm (A260 and A280, respectively) using a SmartSpec Plus Spectrophotometer (Bio-Rad Laboratories, Inc., Hercules, CA, USA). RNA integrity was further verified by electrophoresis using a 1.5% agarose gel. All RNA samples were stored at -80 °C for future analysis. Reverse transcription reactions were carried out using the ReverTra Ace qPCR RT Kit (TOYOBO Life Science, Shanghai, P.R. China), according to the manufacturer's instructions.

#### Quantitative real-time PCR (qRT-PCR)

Expression levels of the ZC3H13 gene were detected by qRT-PCR. The human (species) ACTB gene was used as a control. Specific primers were designed based on cDNA sequences. Primer sequences of ZC3H13 were as follows: 5'-ACATTCATTAGGCTCTGGTGC-3' (forward), 5'-TTCTCCCTCATCCTGTTGGTCC-3' (reverse). qRT-PCR was performed on a Bio-Rad S1000 with Bestar SYBR GreenRT-PCR Master Mix (TOYOBO). PCR conditions consisted of denaturing at 95 °C for 1 min, and 40 cycles of denaturing at 95 °C for 15 s followed by annealing and extension at 60 °C for 30 s. The relative gene expression was calculated using the Livak and Schmittgen 2<sup>-ΔΔC<sub>t</sub></sup> method (Livak and Schmittgen 2001), normalized with the reference gene actin. PCR amplifications were performed in triplicate for each sample.

#### Immunohistochemical analysis

The tissue slides (4-μm-thick sections) were initially treated for deparaffinization, rehydration, and antigen-retrieval using 3% H<sub>2</sub>O<sub>2</sub>. The sections were incubated with anti-ZC3H13 (Bioss, P.R. China) and then with horseradish peroxidase (HRP)-labeled IgG secondary antibodies (Beyotime Institute of Biotechnology,

Shanghai, P.R. China). Fields from each slide were examined and photographed using a light microscope (Olympus, Japan).

#### Western blot analysis

Cells were lysed in a radioimmunoprecipitation assay buffer containing 1 nM phenylmethanesulfonyl fluoride, and protein concentrations were determined using a bicinchoninic acid (BCA) protein assay kit (Biosharp, Guangzhou, China) according to the manufacturer's instructions. Protein samples (40 µg) of each group were boiled with 6 × sodium dodecyl sulfate loading buffer for 10 min before electrophoresis on 12% sodium dodecyl sulfate–polyacrylamide gel electrophoresis gels. The resolved proteins were electrotransferred onto polyvinylidene difluoride membranes (Millipore, Billerica, MA, USA) in a transferring buffer (25 mM Tris, 0.2 M glycine, and 25% methanol). After blocking with 5% skimmed milk, the membranes were incubated with anti-ZC3H13 (Bioss, P.R. China) and anti-β-actin antibodies (Bioss, P.R. China), followed by incubation with appropriate HRP-conjugated secondary antibodies (Abcam, England).

#### Cell transfection

ZC3H13-siRNA (5'-GAAGACAUCUGCAGUAUCU-3', antisense 5'-AGAUACUGCAGAUGUCUUC-3') was synthesized by GeneCreate Bioengineering Co., Ltd. Gene Create (Wuhan, P.R. China). According to the manufacturer's instructions, Lipofectamine 2000 (Invitrogen, USA) was used for transfecting siRNAs into HeLa and SiHa cells.

#### CCK8 assay

Cells were digested with trypsin and inoculated into 96-well plates. The culture plate was placed in a 5% CO<sub>2</sub> incubator for 0, 24, and 48 h at 37°C. Next, rapamycin (GlpBio, USA) and/or FBS (Gibco, USA) were added. Then, the CCK-8 (Solarbio, Beijing, China) solution was added, and the samples were incubated for 0.5 h. The absorbance of each well was measured at 450 nm.

#### Transwell chamber assay

The cell invasion ability was evaluated using Transwell chambers precoated with Matrigel. A total of 1 × 10<sup>4</sup> cells were inoculated into the top chamber and incubated at 37 °C with 5% CO<sub>2</sub> for 48 h. After cells on top of the filter were removed, cells on the bottom of the filter were fixed in 4% paraformaldehyde and stained with 1% crystal violet (Beyotime, P.R. China). The invading cells were counted under a microscope.

#### Wound-healing assay

Approximately 5 × 10<sup>5</sup> HeLa cells were seeded in 6-well plates. The cells were washed with PBS three times, and fresh medium was added. Cells were cultured in a 37 °C 5% CO<sub>2</sub> incubator, photographed, and recorded under the microscope at 0, 24, and 48 h.

#### m<sup>6</sup>A ELISA

The total RNA extracted was detected by EpiQuik™ m<sup>6</sup>A RNA Methylation Quantification Kit (Epigentek, USA), following the manufacturer's instructions.

#### Statistical analysis

All data processing and analysis were completed in R (version 3.6.2). To compare two groups of continuous variables, the statistical significance of the normally distributed variables was estimated using the independent student's t-test, and the differences between non-normally distributed variables were analyzed using the Mann–Whitney U test (i.e., Wilcoxon rank-sum test). The Chi-square test or Fisher's exact test was used to compare and analyze the statistical significance between two groups of categorical variables. The correlation coefficients of different genes were calculated using Pearson correlation analysis. R's survival package was used for survival analysis, the Kaplan–Meier survival curve was used to highlight the survival difference, and the log-rank test was used to evaluate the significance of the survival time difference between two groups [36]. R's pROC package was used to plot the receiver operating characteristic (ROC) curve and calculate the area under the curve (AUC) to assess the accuracy of the risk score in estimating prognosis. Univariate and multivariate Cox analyses were used to determine independent prognostic factors [37]. All statistical P-values were bilateral, and P < 0.05 was considered statistically significant.

## Results

A flow chart of the study is shown in Fig. 1A.

#### Expression and mutation profile of m<sup>6</sup>A-related genes in patients with CESC

To analyze the overall expression of m<sup>6</sup>A-related genes in patients with CESC, we analyzed the genomic mutations and mRNA expression, including single nucleotide polymorphism, CNV, and gene expression level. SNP analysis showed that 37 of 289 samples had single nucleotide mutations in m<sup>6</sup>A-related genes (Fig. 1B). Moreover, studies on the change frequency of CNV showed that the changes of m<sup>6</sup>A-related genes in CNV levels were widespread in patients with CESC, and most were focused on

the loss of copy number. Fig. 1C and D show the position and frequency of CNV changes on chromosomes, respectively.

Next, we comprehensively analyzed the expression of m<sup>6</sup>A-related genes in cervical cancer and cervical tissue in the TCGA database, GTEx database, and GSE52903 dataset, and batch effects were removed. PCA results showed significant differences in overall expression levels between tumor samples and normal tissues after batch removal (Fig. 1E). We focused on m<sup>6</sup>A-related genes and compared the differences of m<sup>6</sup>A-related genes between the two groups by the Wilcoxon rank-sum test. Differential analysis results showed that many m<sup>6</sup>A-related genes were differentially expressed between cervical cancer tissues and normal tissues, including METTL14, METTL16, ZC3H13, YTHDC1, and YTHDC2 (Fig. 1F). After further correlation analysis, a heat map was constructed, which showed the correlation of m<sup>6</sup>A-related gene expression. Most genes showed a positive correlation in CESC tissues (Fig. 1G).

We further selected and analyzed the influence of m<sup>6</sup>A-related genes on the prognosis of patients with CESC based on the TCGA and GEO databases. The gene network depicted a comprehensive picture of m<sup>6</sup>A-related gene interactions, source grouping, and their impact on OS in patients with CESC (Fig. 2A).

Subsequently, we constructed a risk scoring system based on the expression of m<sup>6</sup>A-related genes to quantitatively evaluate the impact of m<sup>6</sup>A-related genes on the prognosis of each patient with CESC. First, 20 m<sup>6</sup>A-related genes were included in the LASSO Cox analysis, and 12 genes with the best prognostic value were selected and identified (Fig. 2B, C). Simultaneously, based on the penalty coefficient of important characteristic genes calculated by LASSO Cox analysis, the gene expression was multiplied and added to the corresponding coefficient to establish the risk score, and the final risk score of each sample was calculated. The significance of the LASSO Cox analysis here was to eliminate the multicollinearity between genes (resulting from the use of LASSO), and ultimately, to ensure that the genes included in the multivariate Cox regression are

independent. The distribution of risk score, survival status, and expression patterns of characteristic genes were shown in Fig. 2D. Kaplan–Meier analysis showed that the OS of patients with high-risk scores was relatively poor (log-rank  $P < 0.001$ ; Fig. 2E). The time-dependent ROC analysis of the risk score showed that the risk score had a good predictive ability for the OS of patients with CESC, and the AUC of 1-, 3-, and 5-year OS were 0.734 (0.642–0.825), 0.702 (0.648–0.797), and 0.723 (0.665–0.829), respectively (Fig. 2F).

### Influence of m<sup>6</sup>A risk score on the biological function of patients with CESC

We then divided patients into high- and low-risk groups based on the median m<sup>6</sup>A risk score for patients with CESC and assessed the changes in biological function between the two groups. To analyze the variation in different pathways in patients with CESC, the enrichment scores of patients with CESC were analyzed using the GSVA method, and the related signaling pathways with significant differential expression in the high- and low-risk patients were shown through heat maps (Fig. 2G). In addition, the analysis revealed significant differences in the enrichment of related biological pathways, such as CD8<sup>+</sup> T cell effectors, immune checkpoints, EMT pathways, and angiogenesis, between high- and low-risk patients ( $P < 0.05$ ; Fig. 2H).

### Construction of genetic characteristics of patients with CESC based on the m<sup>6</sup>A risk model

To determine the underlying biological characteristics of different m<sup>6</sup>A-associated phenotypes, the LIMMA package was used to analyze differential genes between different risk models in the dataset and yielded 207 DEGs. The DEGs are shown in Additional file 2 materials. Subsequently, based on the DEGs, patients with CESC were divided into three different subtypes named Gene-clusters A, B, and C (Fig. 3A) using unsupervised clustering. According to the expression and correlation of DEGs between different groups, genes were divided into m<sup>6</sup>A signature gene-A and B groups. At the same time,

(See figure on next page.)

**Fig. 1** Overall expression of m<sup>6</sup>A-related genes in patients with CESC. **A** Workflow of the study. **B** Mutation map of m<sup>6</sup>A-related genes in TCGA-patients with CESC. Samples were sequenced according to the burden of nonsynonymous mutations in somatic cells, and genes were sequenced according to the mutation frequency. Different colors indicate different mutation types. The section above the legend shows the mutation load; **C** CNV differential changes and locations of m<sup>6</sup>A-related genes on 23 chromosomes of patients with TCGA-CESC; **D** change frequency of CNV level of m<sup>6</sup>A-related genes, where red represents CNV level amplification and green represents CNV level deletion; **E** PCA showed differences between cervical and normal cervical tissues before and after combination and batch effect removal in TCGA, GTEx, and GEO datasets. The left panel shows the result before batch effect removal, and the right shows the result after batch effect removal. **F** Differentially expressed m<sup>6</sup>A-related genes in cervical cancer and normal cervical tissue; **G** expression correlation analysis of m<sup>6</sup>A-related genes in CESC

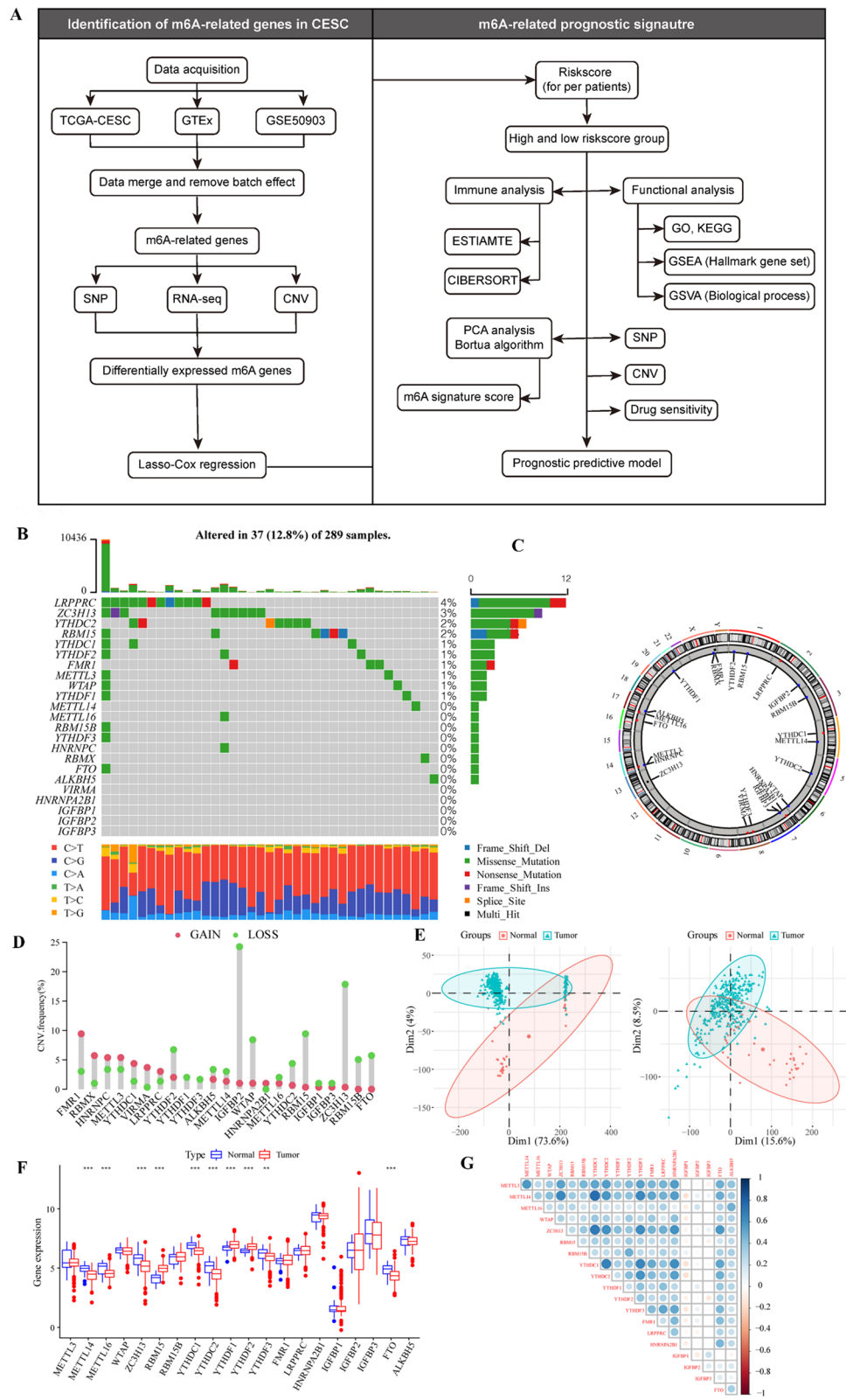


**Fig. 1** (See legend on previous page.)

survival analysis results showed significant differences in the prognosis of patients with three different gene subtypes. Patients in Genecluster A had the worst prognosis (log-rank  $P < 0.001$ ; Fig. 3B).

DEGs were divided into two groups, m<sup>6</sup>A signature-A and m<sup>6</sup>A signature-B, according to the correlation of gene expression. m<sup>6</sup>A signature-A gene set had 101 DEGs, and m<sup>6</sup>A signature-B gene set included 106 DEGs. To explore differences in biological functions between the two groups of genes, functional enrichment analysis was performed (Tables 1 and 2). GO and KEGG enrichment analysis showed that signature-A and -B gene sets showed different unique BPs. Signature-A gene set involved leukotriene catabolic processes, leukotriene B4 catabolic processes, leukotriene B4 metabolic processes, glycosphingolipid biosynthesis-lacto and neolacto series, nicotine addiction, and other pathways (Fig. 3C, D). In contrast, the gene set of overexpressed signature gene-B mainly showed heat generation, positive regulation of angiogenesis, positive regulation of vasculature development, AGE-RAGE signaling pathway in diabetic complications, pertussis, cellular senescence, and other pathways (Fig. 3E, F). The pathways are shown in Additional file 3 materials.

#### Construction of prognostic m<sup>6</sup>A feature model based on m<sup>6</sup>A signature gene

To better predict the impact of m<sup>6</sup>A characteristics on patient prognosis, we constructed a new prognostic-related risk scoring system. According to the expression of m<sup>6</sup>A Signature-A and -B gene sets in patients with CESC, the corresponding PCA1 of m<sup>6</sup>A signature-A and -B gene sets in each patient was calculated by PCA, and the corresponding m<sup>6</sup>A score of each patient

was obtained by subtraction, which was named the m<sup>6</sup>A group. Similarly, patients were divided into high- and low-risk groups based on the median prognostic model scores. The Sankey diagram showed the corresponding gene group (Geneclusters A, B, and C) of each patient with CESC, the prognosis model m<sup>6</sup>A group, and the corresponding relationship among the survival statuses of patients (Fig. 3G). Simultaneously, survival analysis showed that the prognostic score model could accurately predict the OS of patients with CESC (log-rank  $P < 0.001$ ; Fig. 3H).

Subsequently, we analyzed the effect of the high- and low-risk m<sup>6</sup>A group on patients' biology-related functions. GSEA showed that epithelial-mesenchymal transition, angiogenesis, Myc target V1, and other pathways were mainly enriched in the high-risk group (Fig. 3I), whereas bile acid metabolism, KRAS signaling DN, estrogen response late, and other pathways were significantly enriched in low-risk patients (Fig. 3J) (Table 3).

#### Influence of m<sup>6</sup>A risk score on immune characteristics of patients with CESC

Next, we assessed the impact of the m<sup>6</sup>A risk score on the overall immune characteristics and different levels of immune cell infiltration in patients with CESC. The immune score was significantly lower in the high-risk group than in the low-risk group ( $P = 0.025$ , Fig. 4A), whereas the stromal score was not significantly different ( $P = 0.64$ , Fig. 4B). Meanwhile, the CIBERSORT algorithm was further used to evaluate the invasion levels of 22 different immune cells (Fig. 4C). The difference analysis showed that the infiltration levels of various immune cell subsets differed significantly between the high- and low-risk groups (Fig. 4D), including T cells CD8, T cells, CD4 memory activated T cells, follicular helper cells, and M1 macrophages.

(See figure on next page.)

**Fig. 2** Construction of m<sup>6</sup>A risk scoring model and influence of m<sup>6</sup>A risk model on different biological characteristics. **A** Expression and interaction of m<sup>6</sup>A-related genes in patients with CESC. The size of each cell represents the impact of each gene on patient survival, which was analyzed using the logarithmic rank test. The color of one half of the circles represents the m<sup>6</sup>A-related gene group, and the other half represents the effect on prognosis. The m<sup>6</sup>A-related genes were grouped as erasers (red), readers (orange), and writers (gray). Meanwhile, in terms of the impact on prognosis, purple represents risk factors, and green represents protective factors. The lines connecting the m<sup>6</sup>A-related genes represent interactions between genes. The thickness of the line represents the correlation intensity estimated by the Spearman correlation analysis. The positive correlation is represented by red, and the negative correlation is represented by blue. **B, C** LASSO Cox analysis identified 12 genes most associated with TCGA data set OS. **D** Distribution of risk scores for patients with CESC, patient survival, and heat maps of characteristic gene expression; **E** Kaplan–Meier curve analysis to assess the effect of risk score on overall survival in patients with CESC; **F** ROC curve analysis of time dependence of risk score. **G** GSVA analysis of patients in the high- and low-risk subgroups based on gene expression data of patients with CESC. Heat maps were used to demonstrate the relevant pathways with significant differential enrichment. **H** Enrichment of different pathway characteristics (immune-related characteristics, mismatch-related characteristics, and matrix-related characteristics) in the high- and low-risk score subgroups, where thick lines represent the median. The bottom and top of the box are the 25th and 75th percentiles (interquartile spacing) (\* $P < 0.05$ , \*\* $P < 0.01$ , \*\*\* $P < 0.001$ )



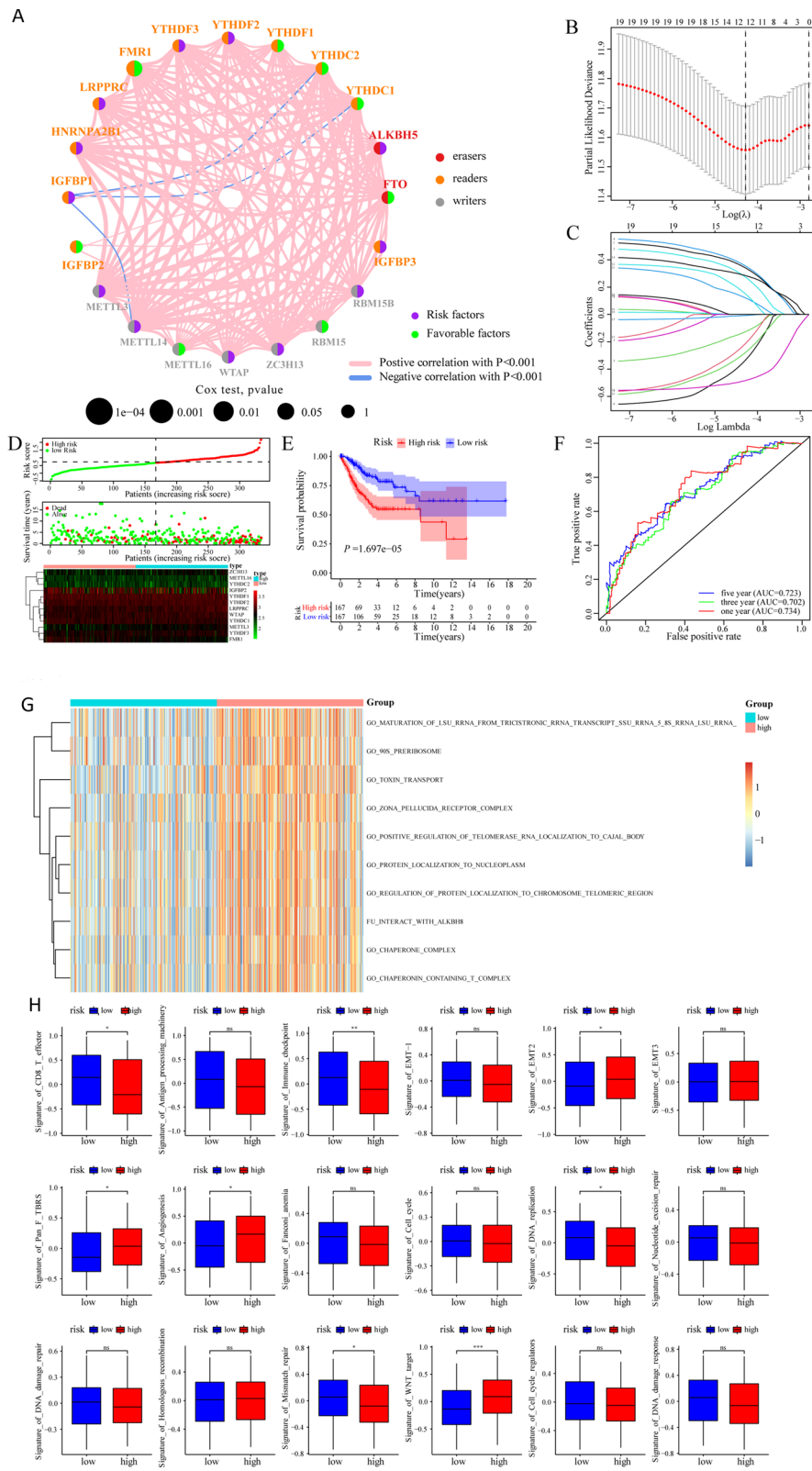


**Fig. 2** (See legend on previous page.)

### Influence of m<sup>6</sup>A risk score on genomic changes in patients with CESC

Subsequently, we further assessed the impact of the m<sup>6</sup>A risk score on changes in levels of genetic variation in patients with CESC, including single nucleotide polymorphism and CNV. Analysis of single nucleotide mutations in driver genes during common tumorigenesis revealed that SNP levels in different driver genes were different between the high- and low-risk subgroups (Fig. 5A). Simultaneously, the overall level analysis showed that the TMB ( $P=0.035$ , Fig. 5B) and tumor neoantigen levels ( $P=0.0079$ , Fig. 5C) significantly differed between the high- and low-risk groups. Moreover, studies on the change frequency of CNV showed that CNV changes in high-risk patients were mainly focused on gene amplification (Fig. 5D), whereas in low-risk patients, CNV changes were mainly manifested as gene copy number deletion (Fig. 5E).

### Sensitivity analysis of patients with CESC to different small molecule drugs based on m<sup>6</sup>A risk score

To analyze the sensitivity of the m<sup>6</sup>A risk score to different drugs and small molecule substances in patients, we downloaded the cell line gene mutation data and IC<sub>50</sub> values of different anticancer drugs from the GDSC database. IC<sub>50</sub> values for patients with CESC were predicted based on the reactivity of cell lines to 138 different chemotherapeutic agents and small molecule anticancer agents. The results showed that the IC<sub>50</sub> values of multiple chemotherapeutic agents and small molecule anticancer agents significantly differed between patients with high and low m<sup>6</sup>A risk scores ( $P<0.001$ ; Fig. 6), especially, KIN001.135, Akt.inhibitor.viii, and rapamycin.

### Construction of the clinical prediction model based on m<sup>6</sup>A risk score

Subsequently, we assessed the impact of the m<sup>6</sup>A risk score on the outcome of patients with CESC. Univariate and multivariate Cox analysis showed that the m<sup>6</sup>A risk score was an independent risk factor for predicting the prognosis of patients with CESC (Fig. 7A). Subsequently, the m<sup>6</sup>A risk score was combined with different clinicopathological features to construct a predictive rosette to predict the OS of patients with CESC (Fig. 7B). The C-index was used to calculate the distinguishing ability of the lipogram, which showed a high degree of differentiation [0.736 (0.680–0.792)]. Moreover, the calibration curves showed a good agreement between the 1-, 3-, and 5-year OS estimates from the rosettes and the actual patient observations (Fig. 7C).

### ZC3H13 expression in tissues

We used qPCR to study ZC3H13 expression in ten normal cervical tissues and ten cervical cancer tissues and found that ZC3H13 was significantly downregulated in cervical cancer tissues (Fig. 8A). The IHC analysis showed that ZC3H13 was localized in the nucleus and had a low expression in cervical cancer tissues (Fig. 8B). We performed gray level difference analysis of IHC results using the Image-Pro Plus software. The results showed that the mean integral optical density (IOD) of ZC3H13 in normal cervical tissues was significantly higher than that of ZC3H13 in cervical cancer tissues. The WB analysis also demonstrated the low expression of ZC3H13 in cervical cancer tissues (Fig. 8C).

### Function of ZC3H13 in cervical cancer and effects of rapamycin on cell phenotypes

The CCK8 assay showed that the proliferation of HeLa and SiHa cells was significantly enhanced after

(See figure on next page.)

**Fig. 3** Construction and functional annotation of the m<sup>6</sup>A gene characteristic model, construction of prognostic m<sup>6</sup>A feature model, and regulation of BPs in patients with CESC. **A** Based on the expression characteristics of DEGs between high and low m<sup>6</sup>A risk scores, unsupervised analysis and hierarchical clustering were performed to classify patients into three categories: Geneclusters A, B, and C, and DEGs were divided into signature -A and -B gene sets according to their expression changes. **B** Survival analysis showed significant differences in prognosis among the different Genecluster groups, and Genecluster A had the worst prognosis. **C** GO analysis showed that signature gene-A was involved in leukotriene catabolic processes, leukotriene B4 catabolic processes, and leukotriene B4 metabolic processes. **D** KEGG analysis showed that the signature-A gene set is closely related to glycosphingolipid biosynthesis-lacto and neolacto series, nicotine addiction, and other pathways. **E** GO analysis showed that the signature-B gene set was involved in heat generation, positive regulation of angiogenesis, and positive regulation of vasculature development. **F** KEGG enrichment analysis showed that signature-B and age-range signaling pathways in diabetic complications, pertussis, cellular senescence, and other pathways are closely related. **G** Sankey plots show correlations between the different gene clusters (Geneclusters A, B, and C, prognostic m<sup>6</sup>A traits (m<sup>6</sup>A group), and patient prognostic status (OS). **H** Survival analysis showed that the prognostic m<sup>6</sup>A feature model could better predict the OS of patients with CESC (log-rank  $P<0.001$ ). **I, J** GSEA for high- and low-risk patients. A signature gene set was downloaded from the MSigDB database, with 1,000 replicates per run. Epithelial-mesenchymal transition, angiogenesis, and Myc targets V1 were mainly enriched in high-risk groups, while bile acid metabolism, KRAS signaling DN, estrogen response late, and other pathways were significantly enriched in low-risk patients

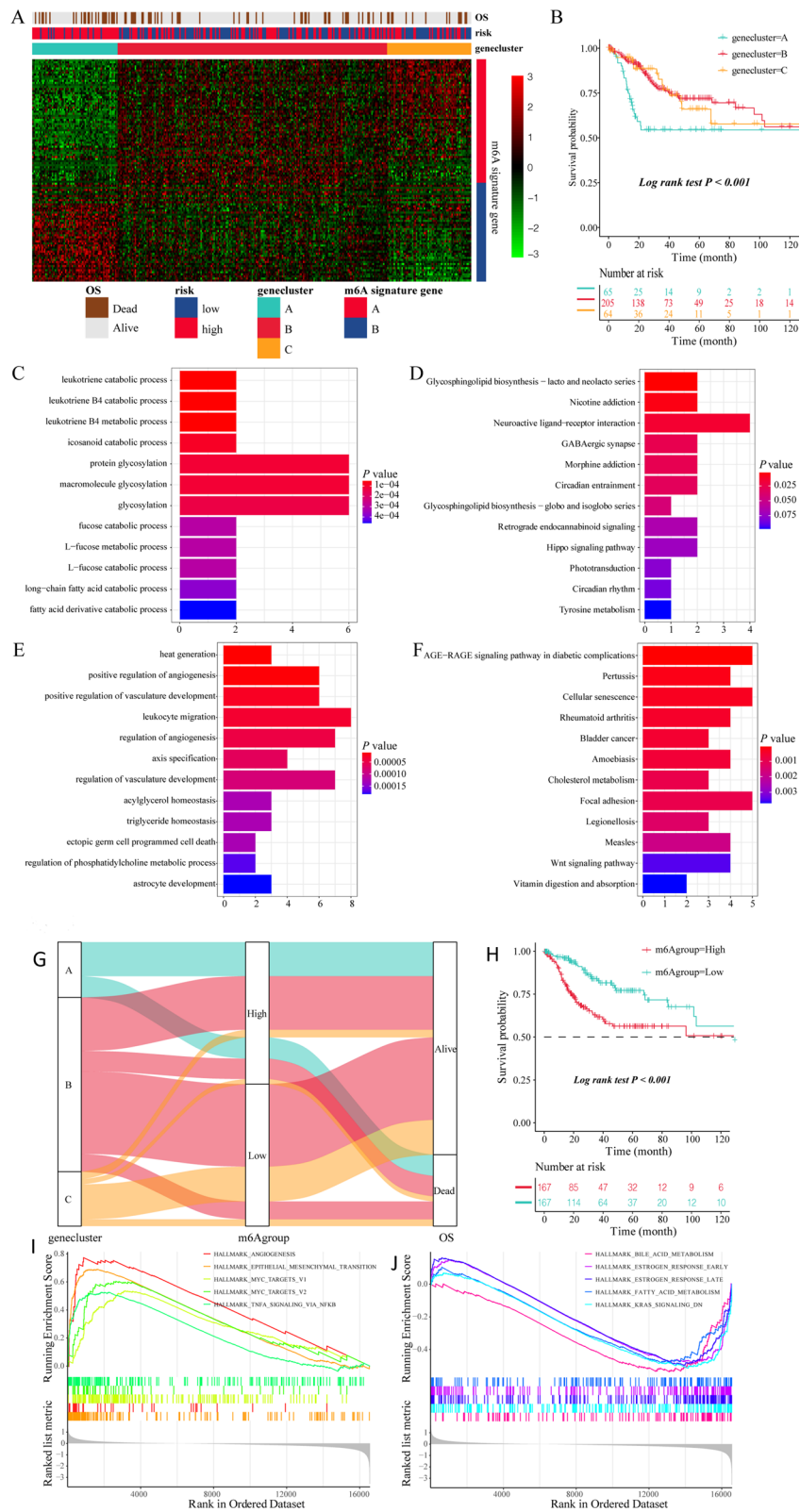


**Fig. 3** (See legend on previous page.)

**Table 1** GO analysis of m6A signature genes

| ONTOLOGY             | ID         | Description  | Count | P value  | Gene   |
|----------------------|------------|--|-------|----------|--|
| m6A Signature gene-A |            |  |       |          |  |
| BP                   | GO:0036100 | leukotriene catabolic process                      | 2     | 5.09E-05 | CYP4F12/CYP4F3                                     |
| BP                   | GO:0036101 | leukotriene B4 catabolic process                   | 2     | 5.09E-05 | CYP4F12/CYP4F3                                     |
| BP                   | GO:0036102 | leukotriene B4 metabolic process                   | 2     | 5.09E-05 | CYP4F12/CYP4F3                                     |
| CC                   | GO:0016324 | apical plasma membrane                             | 7     | 3.52E-05 | CEACAM5/CEACAM6/MUC20/CEACAM7/CYP4F12/SCNN1B/DUOX1 |
| CC                   | GO:0045177 | apical part of cell                                | 7     | 0.000115 | CEACAM5/CEACAM6/MUC20/CEACAM7/CYP4F12/SCNN1B/DUOX1 |
| CC                   | GO:1902711 | GABA-A receptor complex                            | 2     | 0.00136  | GABRP/GABRE  |
| MF                   | GO:0070330 | aromatase activity                                 | 3     | 1.01E-05 | CYP4X1/CYP4F12/CYP4B1                              |
| MF                   | GO:0050051 | leukotriene-B4 20-monooxygenase activity           | 2     | 5.67E-05 | CYP4F12/CYP4F3                                     |
| MF                   | GO:0020037 | heme binding                                       | 5     | 6.14E-05 | CYP4X1/CYP4F12/CYP4F3/DUOX1/CYP4B1                 |
| m6A Signature gene-B |            |  |       |          |  |
| BP                   | GO:0031649 | heat generation                                    | 3     | 9.92E-06 | APLN/IL1B/IL1A                                     |
| BP                   | GO:0045766 | positive regulation of angiogenesis                | 6     | 1.17E-05 | CXCL8/DLL1/ANGPTL4/IL1B/ITGA5/IL1A                 |
| BP                   | GO:1904018 | positive regulation of vasculature development     | 6     | 2.31E-05 | CXCL8/DLL1/ANGPTL4/IL1B/ITGA5/IL1A                 |
| MF                   | GO:0005342 | organic acid transmembrane transporter activity    | 4     | 0.000661 | SLC19A1/SLC6A11/SLC7A5/SLC16A1                     |
| MF                   | GO:0046943 | carboxylic acid transmembrane transporter activity | 4     | 0.000661 | SLC19A1/SLC6A11/SLC7A5/SLC16A1                     |
| MF                   | GO:0005149 | interleukin-1 receptor binding                     | 2     | 0.000775 | IL1B/IL1A  |

**Table 2** KEGG analysis of m6A signature genes

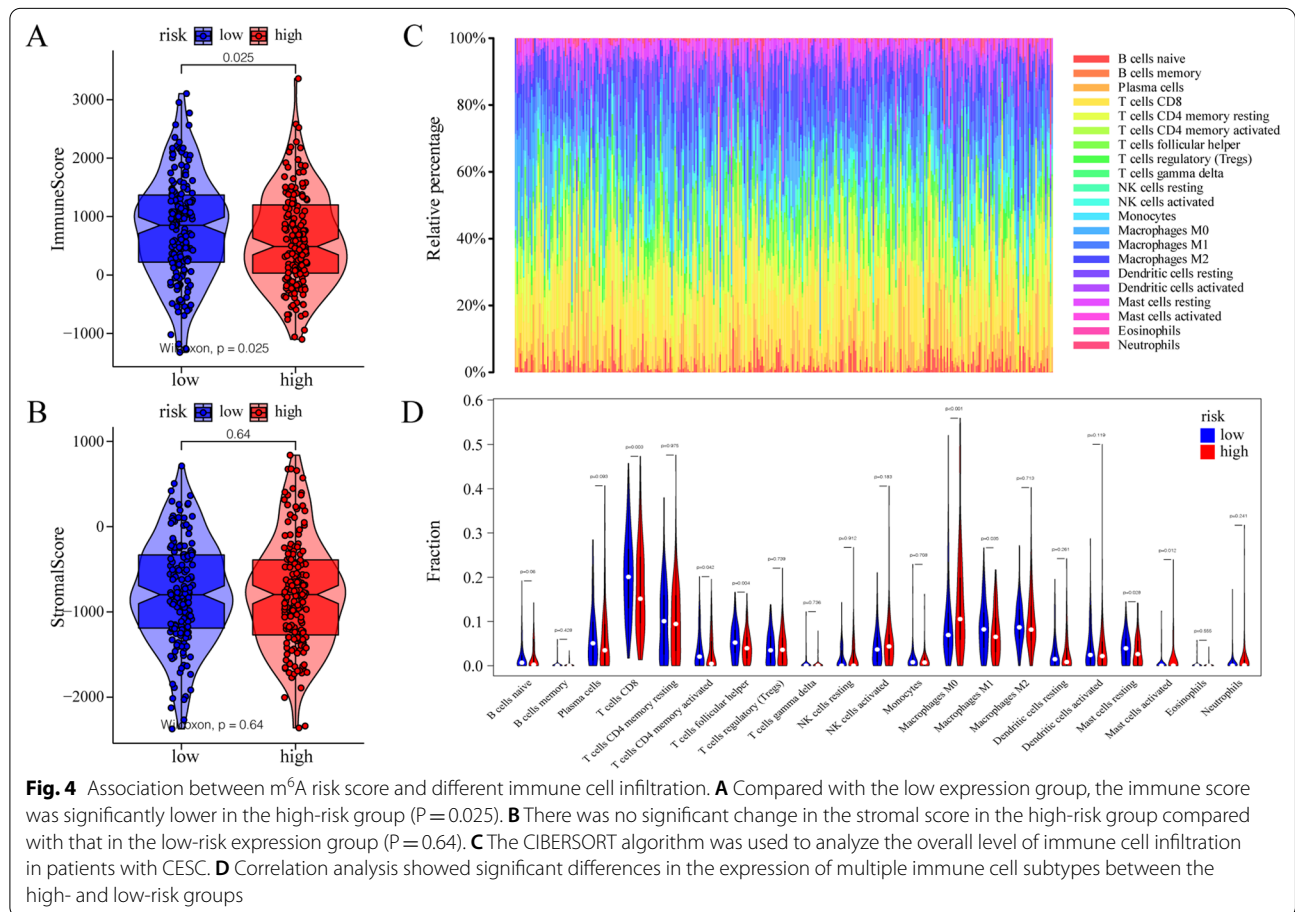
| ID                          | Description  | Count | P value  | Gene                          |
|-----------------------------|--|-------|----------|-------------------------------|
| <b>m6A Signature gene-A</b> |  |       |          |                               |
| hsa00601                    | Glycosphingolipid biosynthesis—lacto and neolacto series | 2     | 0.00259  | FUT2/FUT6                     |
| hsa05033                    | Nicotine addiction                                       | 2     | 0.005628 | GABRP/ GABRE                  |
| hsa04080                    | Neuroactive ligand-receptor interaction                  | 4     | 0.014459 | GABRP/NPW/NMU/GABRE           |
| hsa04727                    | GABAergic synapse  | 2     | 0.025976 | GABRP/GABRE                   |
| hsa05032                    | Morphine addiction                                       | 2     | 0.02707  | GABRP/GABRE                   |
| <b>m6A Signature gene-B</b> |  |       |          |                               |
| hsa04933                    | AGE-RAGE signaling pathway in diabetic complications     | 5     | 3.41E-05 | CXCL8/CCND1/COL4A6/IL1B/ IL1A |
| hsa05133                    | Pertussis  | 4     | 0.000185 | CXCL8/IL1B/ITGA5/IL1A         |
| hsa04218                    | Cellular senescence                                      | 5     | 0.000281 | CXCL8/CCND1/CCND2/MYC/IL1A    |
| hsa05323                    | Rheumatoid arthritis                                     | 4     | 0.000403 | CXCL2/CXCL8/IL1B/IL1A         |
| hsa05219                    | Bladder cancer   | 3     | 0.00049  | CXCL8/CCND1/MYC               |

the ZC3H13 knockdown (Fig. 8D). Further, the CCK8 assay showed a significant reduction in the proliferation of HeLa and SiHa cells after rapamycin treatment (Fig. 8E). The wound-healing assay showed that ZC3H13 knockdown significantly enhanced the invasion ability of HeLa and SiHa cells (Fig. 8F). Transwell experiments showed that ZC3H13 knockdown significantly enhanced the cell migration ability (Fig. 8G). The

wound-healing assay showed a significant reduction in the invasion abilities of HeLa and SiHa cells after rapamycin treatment (Fig. 8F). The Transwell assay showed a significant reduction in the migration abilities of HeLa and SiHa cells after rapamycin treatment (Fig. 8G). The m<sup>6</sup>A ELISA showed that the m<sup>6</sup>A levels decreased significantly after the ZC3H13 knockdown (Fig. 8H) and that the m<sup>6</sup>A levels increased significantly

**Table 3** GSEA analysis results

| Name                                       | Size | Enrichment Score | NES      | P value  | Leading edge                         |
|--|------|------------------|----------|----------|--------------------------------------|
| HALLMARK_EPITHELIAL_MESENCHYMAL_TRANSITION | 193  | 0.690003         | 3.006838 | 2.12E-33 | tags = 56%, list = 10%, signal = 51% |
| HALLMARK_ANGIOGENESIS                      | 34   | 0.773029         | 2.613681 | 3.62E-09 | tags = 44%, list = 5%, signal = 42%  |
| HALLMARK_MYC_TARGETS_V1                    | 187  | 0.535557         | 2.344755 | 8.78E-16 | tags = 48%, list = 19%, signal = 39% |
| HALLMARK_MYC_TARGETS_V2                    | 54   | 0.60481          | 2.295545 | 1.48E-06 | tags = 59%, list = 16%, signal = 50% |
| HALLMARK_ESTROGEN_RESPONSE_EARLY           | 187  | -0.4833          | -1.50217 | 0.000929 | tags = 33%, list = 12%, signal = 29% |
| HALLMARK_ESTROGEN_RESPONSE_LATE            | 188  | -0.49748         | -1.54745 | 0.000127 | tags = 43%, list = 16%, signal = 36% |
| HALLMARK_KRAS_SIGNALING_DN                 | 191  | -0.51553         | -1.60538 | 1.91E-05 | tags = 29%, list = 15%, signal = 25% |
| HALLMARK_BILE_ACID_METABOLISM              | 111  | -0.53704         | -1.61638 | 0.000452 | tags = 41%, list = 21%, signal = 32% |



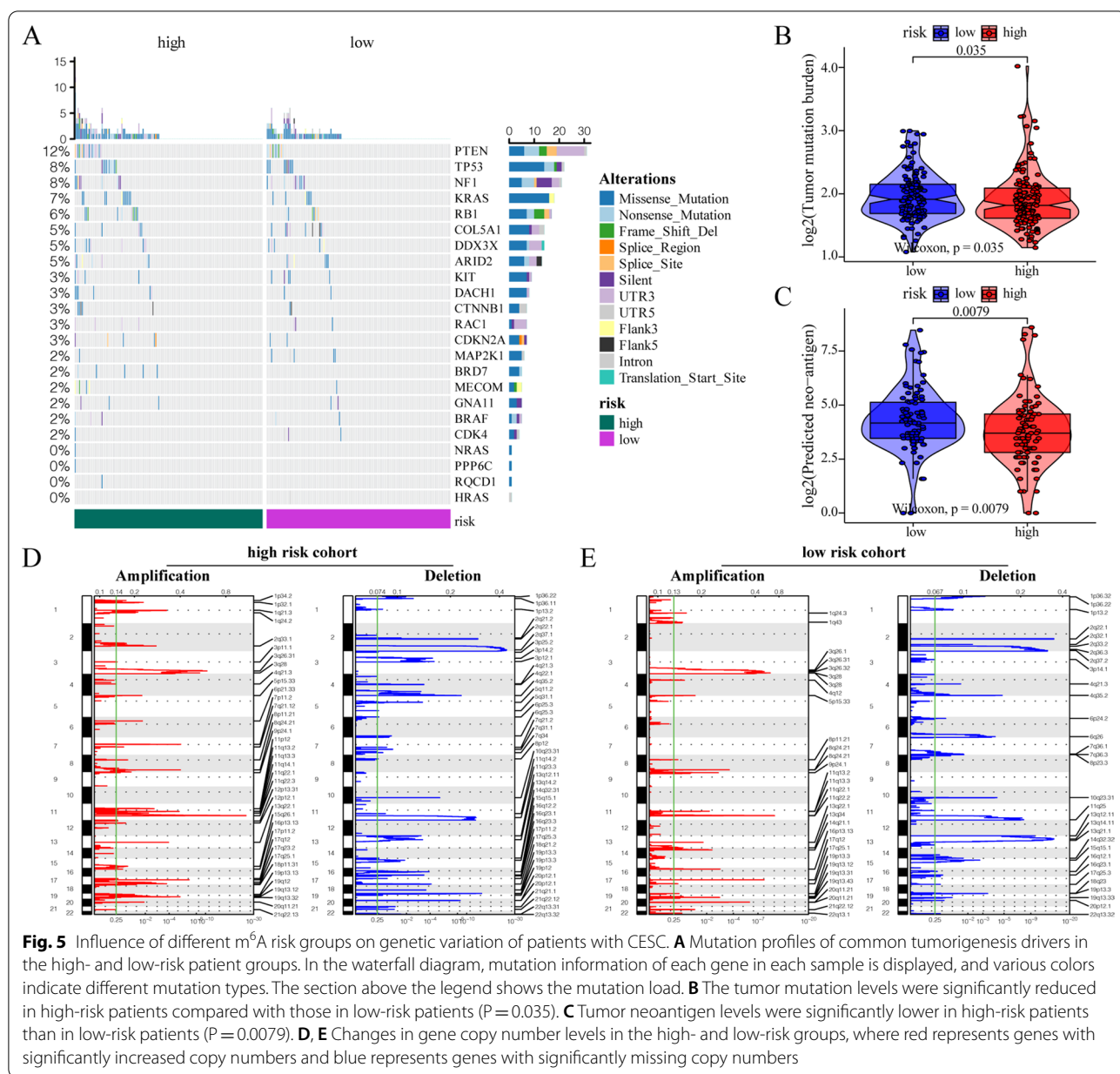


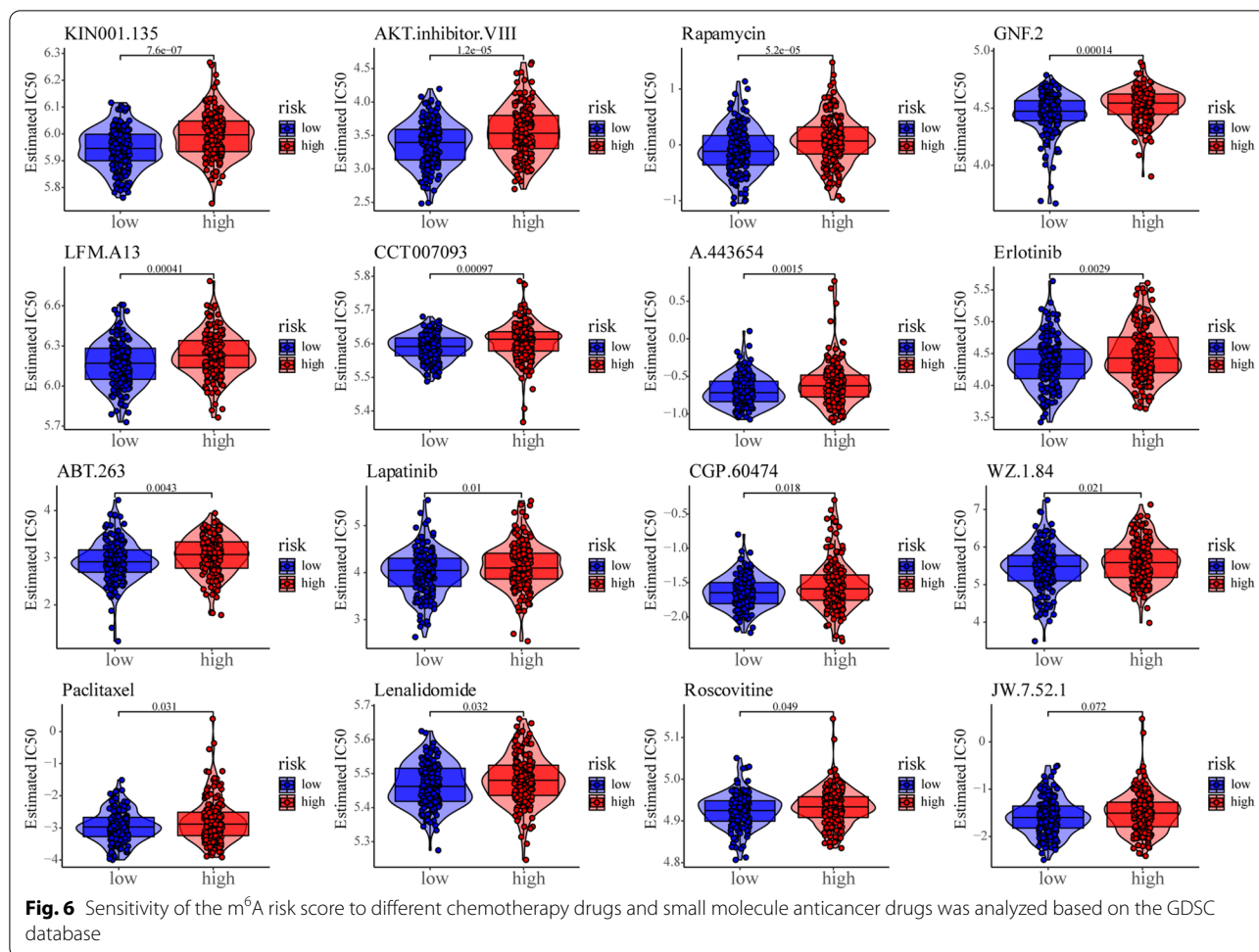
**Fig. 5** Influence of different m<sup>6</sup>A risk groups on genetic variation of patients with CESC. **A** Mutation profiles of common tumorigenesis drivers in the high- and low-risk patient groups. In the waterfall diagram, mutation information of each gene in each sample is displayed, and various colors indicate different mutation types. The section above the legend shows the mutation load. **B** The tumor mutation levels were significantly reduced in high-risk patients compared with those in low-risk patients ( $P = 0.035$ ). **C** Tumor neoantigen levels were significantly lower in high-risk patients than in low-risk patients ( $P = 0.0079$ ). **D, E** Changes in gene copy number levels in the high- and low-risk groups, where red represents genes with significantly increased copy numbers and blue represents genes with significantly missing copy numbers

in both HeLa and SiHa cells after rapamycin treatment (Fig. 8I).

### Discussion

As one of the most common RNA modifications, m<sup>6</sup>A mRNA methylation is closely associated with cervical cancer. m<sup>6</sup>A mRNA methylation might promote cervical cancer development. The m<sup>6</sup>A level was significantly reduced in cervical cancer compared to adjacent

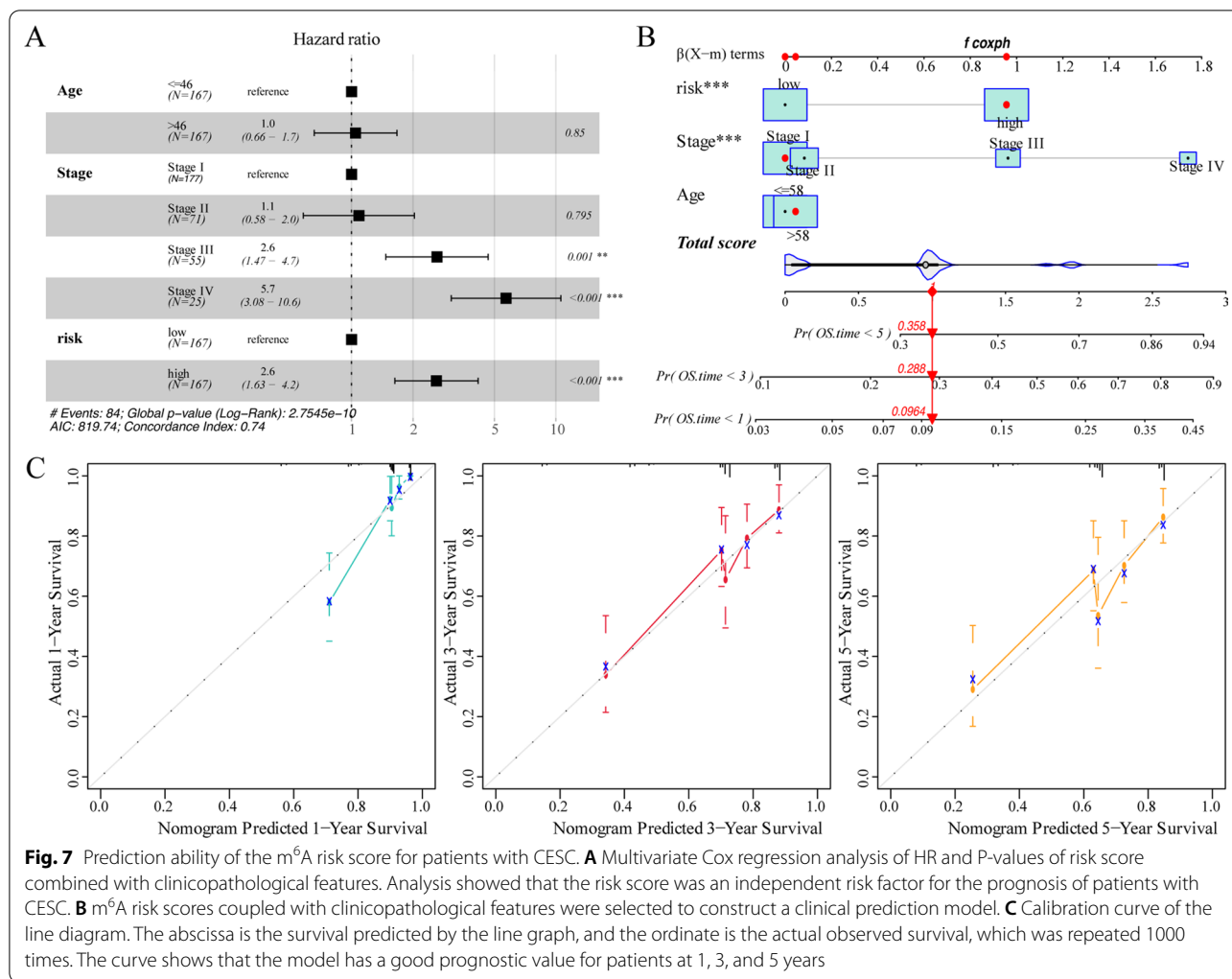
normal tissue. The reduction in m<sup>6</sup>A levels significantly correlated with the FIGO stage, tumor size, differentiation, lymph invasion, and cancer recurrence [38]. m<sup>6</sup>A methyltransferase methyltransferase-like 3 (METTL3) enhanced the stability of FOXD2-AS1, and its expression was maintained. METTL3/FOXD2-AS1 accelerated cervical cancer progression via an m<sup>6</sup>A-dependent modality [39]. METTL3 enhanced the HK2 stability through YTHDF1-mediated m<sup>6</sup>A modification, thereby



promoting the Warburg effect in cervical cancer [40]. GAS5-AS1 interacted with the tumor suppressor GAS5 and increased its stability by interacting with RNA demethylase ALKBH5 and decreasing GAS5 m<sup>6</sup>A modification. m<sup>6</sup>A-mediated GAS5 RNA degradation relied on the m<sup>6</sup>A reader protein YTHDF2-dependent pathway [41]. FTO can control the m<sup>6</sup>A modification of E2F1 and Myc transcripts to regulate the proliferation and migration of cervical cancer cells [42]. The FTO-mediated stabilization of HOXC13-AS epigenetically upregulated FZD6 and activated Wnt/ $\beta$ -catenin signaling, driving CC proliferation, invasion, and EMT [43]. FTO and its substrate m<sup>6</sup>A may be critical factors for regulating chemo-radiotherapy resistance [44]. YTHDF1 regulated the translation of RANBP2, which potentiated the growth, migration, and invasion of cervical cancer cells

in an m<sup>6</sup>A-dependent manner without any effect on its mRNA expression [45]. circARHGAP12 exerted the oncogenic role in cervical cancer progression through the m<sup>6</sup>A-dependent IGF2BP2/FOXO1 pathway [46]. KCNMB2-AS1 and IGF2BP3 formed a positive regulatory circuit that increased the tumorigenic effect of KCNMB2-AS1 in cervical cancer [47]. m<sup>6</sup>A-associated downregulation of miR-193b promoted cervical cancer aggressiveness by targeting CCND1 [48]. ZFAS1 and its m<sup>6</sup>A modification may be a promising target for cervical cancer treatment [49].

According to our study, differential analysis results showed differences in the expression of multiple m<sup>6</sup>A-related genes between cervical cancer tissues and normal tissues; furthermore, these genes were related to prognosis. The established m<sup>6</sup>A risk scoring system



is closely related to the biological function of cervical cancer, immune invasion of cervical cancer, and sensitivity to small molecule drugs. The model based on the m<sup>6</sup>A signature genes and the model based on the m<sup>6</sup>A risk score can accurately predict the prognosis of patients with cervical cancer. Studies showed that m<sup>6</sup>A was closely related to epithelial-mesenchymal transition, angiogenesis, Myc targets V1, KRAS signal pathway, and estrogen in the occurrence and development of tumors [43, 50–54]. Our results showed that epithelial-mesenchymal transition, angiogenesis, Myc targets V1, and other pathways are mainly enriched in

the high-risk groups, while bile acid metabolism, KRAS signaling DN, late estrogen response, and other pathways are significantly enriched in low-risk patients. The results of the present study may help understand the relationship between these pathways and m<sup>6</sup>A, revealing their mechanism in cervical cancer occurrence and development. We also showed that the m<sup>6</sup>A regulator correlates with the survival and clinicopathological characteristics of patients with CESC. The m<sup>6</sup>A regulator-based prognostic signature may predict the prognosis of CESC [55].



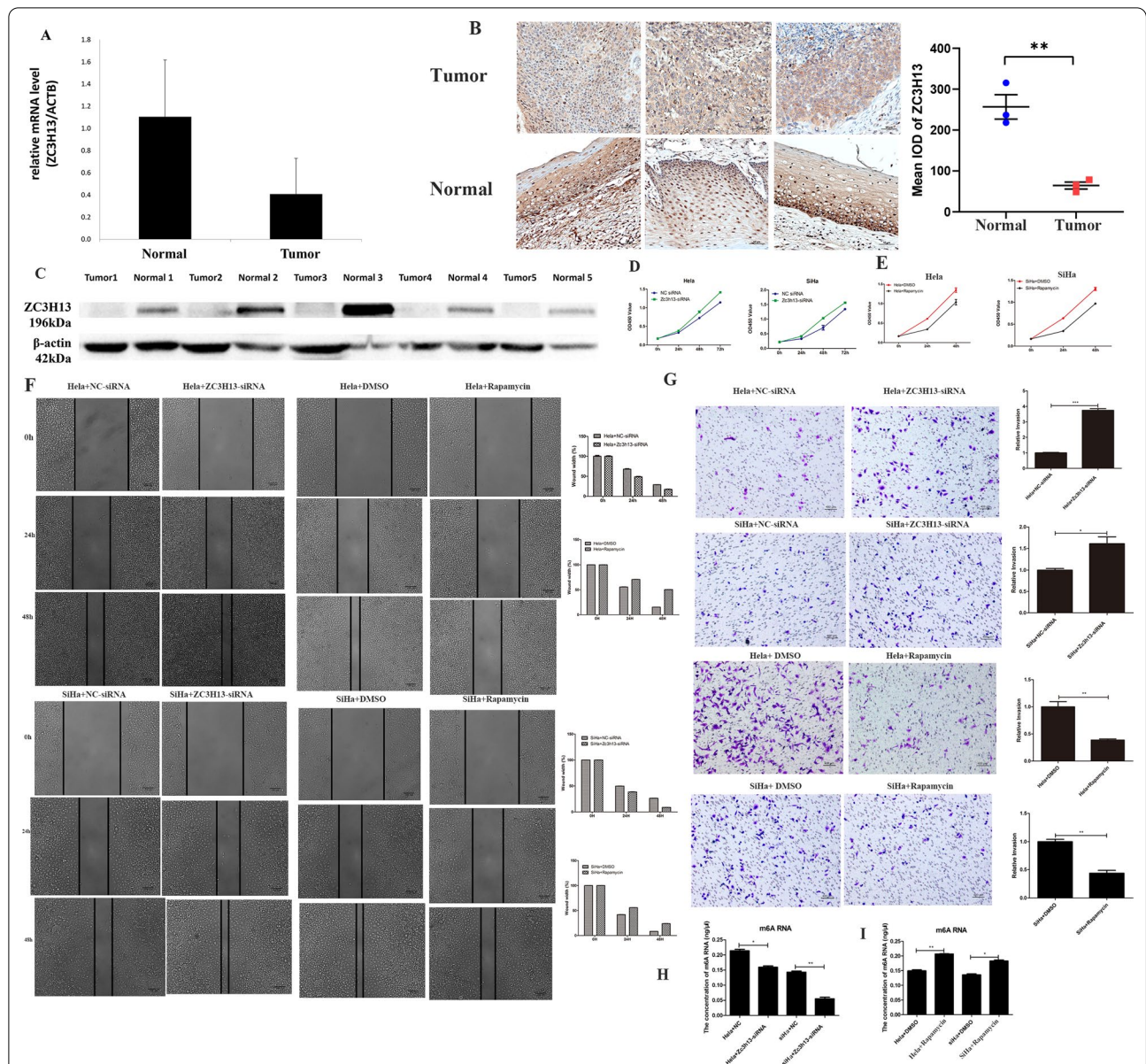


**Fig. 8** Expression and function of ZC3H13 in cervical cancer and the effects of rapamycin on cell phenotypes. **A** The qPCR analyses showed that ZC3H13 was significantly downregulated in cervical cancer tissues ( $P = 0.0019$ ). **B** The IHC analysis showed that ZC3H13 was localized in the nucleus and was expressed at low levels in cervical cancer tissues ( $\times 20$ ) (scale bar: 50  $\mu\text{m}$ ). Gray level difference analysis showed that the IOD of ZC3H13 in normal cervical tissues was significantly higher than that in cervical cancer tissues. **C** The WB analysis demonstrated the low expression of ZC3H13 in cervical cancer tissues. **D** The CCK8 assay showed that the proliferation ability of HeLa and SiHa cells was significantly enhanced after ZC3H13 knockdown. **E** The CCK8 assay showed that the proliferation ability of HeLa and SiHa cells was significantly reduced after rapamycin treatment. **F** The wound-healing assay showed that ZC3H13 knockdown significantly enhanced the invasion abilities of the HeLa and SiHa cells. The wound-healing assay showed that the invasion ability of HeLa and SiHa cells was significantly reduced after rapamycin treatment. **G** The Transwell experiments showed that ZC3H13 knockdown significantly enhanced the migration abilities of the cells. The Transwell assay showed that the migration ability of HeLa and SiHa cells was significantly reduced after rapamycin treatment. **H** The m<sup>6</sup>A ELISA analyses showed that the m<sup>6</sup>A levels decreased significantly after the ZC3H13 knockdown. **I** The m<sup>6</sup>A ELISA analyses showed that the m<sup>6</sup>A levels increased significantly in both HeLa and SiHa cells after rapamycin treatment. All experiments were repeated at least three times (\* $P < 0.05$ , \*\* $P < 0.01$ , \*\*\* $P < 0.001$ )

According to our analysis, the  $IC_{50}$  of multiple chemotherapy drugs differed significantly between patients with high and low  $m^6A$  risk scores. Meanwhile, previous studies have also shown a close relationship between  $m^6A$ , mTOR pathway, and rapamycin. mTORC1 could stimulate oncogenic signaling and control anabolic cell growth via  $m^6A$  [56, 57].  $m^6A$  has been reported to play a fundamental role in the function of the mTOR pathway in gastrointestinal cancer [58]. Reductions in the  $m^6A$  levels increased the expression of mTORC2 in endometrial cancer [59]. The FTO protein was reported to participate in tumorigenesis via interactions with the target of the mammalian target protein Rapamycin (mTOR) [60]. METTL3 was shown to cause the activation of mTORC1 signaling and colorectal cancer development in an  $m^6A$ -dependent manner [61]. Rapamycin may regulate the  $m^6A$  levels and affect the biological characteristics of OSCC cells [62]. METTL3-high tumors showed more sensitivity to everolimus, a rapamycin analog, in gastric cancer [63].

Our study showed that knocking down ZC3H13, an  $m^6A$  methyltransferase, can promote the proliferation, migration, and invasion abilities of cervical cancer cells and reduce the  $m^6A$  levels. Rapamycin suppresses the proliferation, migration, and invasion abilities of cancer cells and can enhance the  $m^6A$  levels, demonstrating the role of the  $m^6A$  methylation modulator in the development of cervical cancer and the effectiveness of the drugs targeting the modulators of  $m^6A$  methylation in treating cervical cancer.

In conclusion, our study shows that  $m^6A$  regulatory factors are closely related to the occurrence, development, immune invasion, drug sensitivity, and prognosis of cervical cancer. Drugs targeting the factors regulating  $m^6A$  offer good prospects for treating cervical cancer.

### Supplementary Information

The online version contains supplementary material available at <https://doi.org/10.1186/s12967-022-03600-7>.

**Additional file 1.** Table of demographic and clinical characteristics of patients with cervical cancer.

**Additional file 2.** DEGs between different risk models.

**Additional file 3.** Pathways of different groups.

### Acknowledgements

The study was supported by the Clinical Medical Research Center of Gynecology and Obstetrical Diseases (gynecological tumors) of Henan Province.

### Author contributions

XL and WW were responsible for designing the study, writing the manuscript, extracting and analyzing data, and interpreting the results. YY and RL were responsible for the experiments. WZ contributed to reviewing and editing the article. All authors read and approved the final manuscript.

### Funding

This work was supported by the Department of science and technology of Henan Province (grant nos. 212102310466 and 182102410095), the Department of Education of Henan Province (grant no. 2019GGJS004), and the Henan Provincial Health Commission (grant no. SBGJ202002119).

### Availability of data and materials

The datasets used or analyzed during the current study are available from the TCGA GDC website (<https://portal.gdc.cancer.gov/>).

### Declarations

#### Ethics approval and consent to participate

This study was performed in accordance with the Helsinki Declaration and approved by the ethics committee of the Second Affiliated Hospital of Zhengzhou University.

#### Consent for publication

Not applicable.

#### Competing interests

The authors declare no conflict of interest.

Received: 19 April 2022 Accepted: 18 August 2022

Published online: 04 September 2022

### References

- Bray F, Ferlay J, Soerjomataram I, et al. Global cancer statistics 2018: GLOBOCAN estimates of incidence and mortality worldwide for 36 cancers in 185 countries. *CA Cancer J Clin*. 2018;68:394–424. <https://doi.org/10.3322/caac.21492>.
- Sung H, Ferlay J, Siegel RL, et al. Global cancer statistics 2020: GLOBOCAN estimates of incidence and mortality worldwide for 36 cancers in 185 countries. *CA Cancer J Clin*. 2021;71:209–49. <https://doi.org/10.3322/caac.21660>.
- Gultekin M, Ramirez PT, Broutet N, Hutubessy R. World Health Organization call for action to eliminate cervical cancer globally. *Int J Gynecol Cancer*. 2020;30:426–7. <https://doi.org/10.1136/ijgc-2020-001285>.
- Delaunay S, Frye M. RNA modifications regulating cell fate in cancer. *Nat Cell Biol*. 2019;21:552–9. <https://doi.org/10.1038/s41556-019-0319-0>.
- Helm M, Motorin Y. Detecting RNA modifications in the epitranscriptome: predict and validate. *Nat Rev Genet*. 2017;18:275–91. <https://doi.org/10.1038/nrg.2016.169>.
- Harcourt EM, Kietrys AM, Kool ET. Chemical and structural effects of base modifications in messenger RNA. *Nature*. 2017;541:339–46. <https://doi.org/10.1038/nature21351>.
- Roundtree IA, Evans ME, Pan T, He C. Dynamic RNA modifications in gene expression regulation. *Cell*. 2017;169(7):1187–200. <https://doi.org/10.1016/j.cell.2017.05.045>.
- He L, Li H, Wu A, et al. Functions of N6-methyladenosine and its role in cancer. *Mol Cancer*. 2019;18:176. <https://doi.org/10.1186/s12943-019-1109-9>.
- Boccalletto P, Machnicka MA, Purta E, et al. MODOMICS: a database of RNA modification pathways. *Nucleic Acids Res*. 2018;46:D303–d7. <https://doi.org/10.1093/nar/gkx1030>.
- Sun T, Wu R, Ming L. The role of  $m^6A$  RNA methylation in cancer. *Biomedicine & pharmacotherapy = Biomedicine & pharmacotherapie*. 2019;112:108613. <https://doi.org/10.1016/j.biopha.2019.108613>.
- Zhou Y, Kong Y, Fan W, et al. Principles of RNA methylation and their implications for biology and medicine. *Biomedicine & pharmacotherapy = Biomedicine & pharmacotherapie*. 2020;131:110731. <https://doi.org/10.1016/j.biopha.2020.110731>.
- Zhou J, Wang J, Hong B, et al. Gene signatures and prognostic values of  $m^6A$  regulators in clear cell renal cell carcinoma—a retrospective study using TCGA database. *Aging*. 2019;11:1633–47. <https://doi.org/10.18632/aging.101856>.

13. Tu Z, Wu L, Wang P, et al. N6-methyladenosine-related lncRNAs are potential biomarkers for predicting the overall survival of lower-grade glioma patients. *Front Cell Dev Biol.* 2020;8:642. <https://doi.org/10.3389/fcell.2020.00642>.
14. Yang G, Sun Z, Zhang N. Reshaping the role of m6A modification in cancer transcriptome: a review. *Cancer Cell Int.* 2020;20:353. <https://doi.org/10.1186/s12935-020-01445-y>.
15. Chandola U, Das R, Panda B. Role of the N6-methyladenosine RNA mark in gene regulation and its implications on development and disease. *Brief Funct Genomics.* 2015;14:169–79. <https://doi.org/10.1093/bfpg/elu039>.
16. Yang J, Chen J, Fei X, et al. N6-methyladenine RNA modification and cancer. *Oncol Lett.* 2020;20:1504–12. <https://doi.org/10.3892/ol.2020.11739>.
17. Alblas M, Velt KB, Pashayan N, et al. Prediction models for endometrial cancer for the general population or symptomatic women: a systematic review. *Crit Rev Oncol Hematol.* 2018;126:92–9. <https://doi.org/10.1016/j.critrevonc.2018.03.023>.
18. Nebbioso A, Tambaro FP, Dell'Aversana C, Altucci L. Cancer epigenetics: moving forward. *PLoS Genet.* 2018;14:e1007362. <https://doi.org/10.1371/journal.pgen.1007362>.
19. Xu Z, Peng B, Cai Y, et al. N6-methyladenosine RNA modification in cancer therapeutic resistance: current status and perspectives. *Biochem Pharmacol.* 2020;182: 114258. <https://doi.org/10.1016/j.bcp.2020.114258>.
20. Ma J, Yang D, Ma XX. Immune infiltration-related N6-methyladenosine RNA methylation regulators influence the malignancy and prognosis of endometrial cancer. *Aging.* 2021;13:16287–315. <https://doi.org/10.18632/aging.203157>.
21. Zhang H, Meltzer P, Davis S. RCircos: an R package for Circos 2D track plots. *BMC Bioinformatics.* 2013;14:244. <https://doi.org/10.1186/1471-2105-14-244>.
22. Mayakonda A, Lin DC, Assenov Y, et al. Maftools: efficient and comprehensive analysis of somatic variants in cancer. *Genome Res.* 2018;28:1747–56. <https://doi.org/10.1101/gr.239244.118>.
23. Medina-Martinez I, Barrón V, Roman-Bassaura E, et al. Impact of gene dosage on gene expression, biological processes and survival in cervical cancer: a genome-wide follow-up study. *PLoS ONE.* 2014;9: e97842. <https://doi.org/10.1371/journal.pone.0097842>.
24. Ritchie ME, Phipson B, Wu D, et al. limma powers differential expression analyses for RNA-sequencing and microarray studies. *Nucleic Acids Res.* 2015;43: e47. <https://doi.org/10.1093/nar/gkv007>.
25. Chen S, Yang D, Lei C, et al. Identification of crucial genes in abdominal aortic aneurysm by WGCNA. *PeerJ.* 2019;7: e7873. <https://doi.org/10.7717/peerj.7873>.
26. Yu G, Wang LG, Han Y, He QY. clusterProfiler: an R package for comparing biological themes among gene clusters. *OMICS.* 2012;16:284–7. <https://doi.org/10.1089/omi.2011.0118>.
27. Subramanian A, Tamayo P, Mootha VK, et al. Gene set enrichment analysis: a knowledge-based approach for interpreting genome-wide expression profiles. *Proc Natl Acad Sci U S A.* 2005;102:15545–50. <https://doi.org/10.1073/pnas.0506580102>.
28. Mariathasan S, Turley SJ, Nickles D, et al. TGFβ attenuates tumour response to PD-L1 blockade by contributing to exclusion of T cells. *Nature.* 2018;554:544–8. <https://doi.org/10.1038/nature25501>.
29. Rosenberg JE, Hoffman-Censits J, Powles T, et al. Atezolizumab in patients with locally advanced and metastatic urothelial carcinoma who have progressed following treatment with platinum-based chemotherapy: a single-arm, multicentre, phase 2 trial. *Lancet.* 2016;387:1909–20. [https://doi.org/10.1016/S0140-6736\(16\)00561-4](https://doi.org/10.1016/S0140-6736(16)00561-4).
30. Şenbabaoğlu Y, Gejman RS, Winer AG, et al. Tumor immune microenvironment characterization in clear cell renal cell carcinoma identifies prognostic and immunotherapeutically relevant messenger RNA signatures. *Genome Biol.* 2016;17:231. <https://doi.org/10.1186/s13059-016-1092-z>.
31. Wilkerson MD, Hayes DN. ConsensusClusterPlus: a class discovery tool with confidence assessments and item tracking. *Bioinformatics.* 2010;26:1572–3. <https://doi.org/10.1093/bioinformatics/btq170>.
32. Newman AM, Liu CL, Green MR, et al. Robust enumeration of cell subsets from tissue expression profiles. *Nat Methods.* 2015;12:453–7. <https://doi.org/10.1038/nmeth.3337>.
33. Yoshihara K, Shahmoradgol M, Martínez E, et al. Inferring tumour purity and stromal and immune cell admixture from expression data. *Nat Commun.* 2013;4:2612. <https://doi.org/10.1038/ncomms3612>.
34. Yang W, Soares J, Greninger P, et al. Genomics of Drug Sensitivity in Cancer (GDSC): a resource for therapeutic biomarker discovery in cancer cells. *Nucleic Acids Res.* 2013;41:D955–61. <https://doi.org/10.1093/nar/gks1111>.
35. Geeleher P, Cox N, Huang RS. pRRophetic: an R package for prediction of clinical chemotherapeutic response from tumor gene expression levels. *PLoS ONE.* 2014;9: e107468. <https://doi.org/10.1371/journal.pone.0107468>.
36. Zeng L, Fan X, Wang X, et al. bioinformatics analysis based on multiple databases identifies hub genes associated with hepatocellular carcinoma. *Curr Genomics.* 2019;20:349–61. <https://doi.org/10.2174/1389202920666191011092410>.
37. Robin X, Turck N, Hainard A, et al. pROC: an open-source package for R and S+ to analyze and compare ROC curves. *BMC Bioinformatics.* 2011;12:77. <https://doi.org/10.1186/1471-2105-12-77>.
38. Wang X, Li Z, Kong B, et al. Reduced m(6A) mRNA methylation is correlated with the progression of human cervical cancer. *Oncotarget.* 2017;8:98918–30. <https://doi.org/10.18632/oncotarget.22041>.
39. Ji F, Lu Y, Chen S, et al. m(6A) methyltransferase METTL3-mediated lncRNA FOXD2-AS1 promotes the tumorigenesis of cervical cancer. *Molecular therapy oncolytics.* 2021;22:574–81. <https://doi.org/10.1016/j.omto.2021.07.004>.
40. Wang Q, Guo X, Li L, et al. N(6)-methyladenosine METTL3 promotes cervical cancer tumorigenesis and Warburg effect through YTHDF1/HK2 modification. *Cell Death Dis.* 2020;11:911. <https://doi.org/10.1038/s41419-020-03071-y>.
41. Ma X, Li Y, Wen J, Zhao Y. m6A RNA methylation regulators contribute to malignant development and have a clinical prognostic effect on cervical cancer. *Am J Trans Res.* 2020;12:8137–46.
42. Zou D, Dong L, Li C, et al. The m(6A) eraser FTO facilitates proliferation and migration of human cervical cancer cells. *Cancer Cell Int.* 2019;19:321. <https://doi.org/10.1186/s12935-019-1045-1>.
43. Wang T, Li W, Ye B, et al. FTO-stabilized lncRNA HOXC13-AS epigenetically upregulated FZD6 and activated Wnt/β-catenin signaling to drive cervical cancer proliferation, invasion, and EMT. *J BUON.* 2021;26:1279–91.
44. Zhou S, Bai ZL, Xia D, et al. FTO regulates the chemo-radiotherapy resistance of cervical squamous cell carcinoma (CSCC) by targeting β-catenin through mRNA demethylation. *Mol Carcinog.* 2018;57:590–7. <https://doi.org/10.1002/mc.22782>.
45. Wang H, Luo Q, Kang J, et al. YTHDF1 aggravates the progression of cervical cancer through m(6A)-Mediated Up-Regulation of RANBP2. *Front Oncol.* 2021;11: 650383. <https://doi.org/10.3389/fonc.2021.650383>.
46. Ji F, Lu Y, Chen S, et al. IGF2BP2-modified circular RNA circARHGAP12 promotes cervical cancer progression by interacting m(6A)/FOXO1 manner. *Cell Death Discovery.* 2021;7:215. <https://doi.org/10.1038/s41420-021-00595-w>.
47. Zhang Y, Wang D, Wu D, et al. Long Noncoding RNA KCNMB2-AS1 Stabilized by N(6)-methyladenosine modification promotes cervical cancer growth through acting as a competing endogenous RNA. *Cell Transplant.* 2020;29:963689720964382. <https://doi.org/10.1177/0963689720964382>.
48. Huang C, Liang J, Lin S, et al. N(6)-Methyladenosine associated silencing of miR-193b promotes cervical cancer aggressiveness by targeting CCND1. *Front Oncol.* 2021;11: 666597. <https://doi.org/10.3389/fonc.2021.666597>.
49. Yang Z, Ma J, Han S, et al. ZFAS1 exerts an oncogenic role via suppressing miR-647 in an m(6A)-dependent manner in cervical cancer. *Oncotargets Ther.* 2020;13:11795–806. <https://doi.org/10.2147/OTT.S274492>.
50. Li J, Xie G, Tian Y, et al. RNA m 6 A methylation regulates dissemination of cancer cells by modulating expression and membrane localization of β-catenin. *Mol Ther.* 2022. <https://doi.org/10.1016/j.jymthe.2022.01.019>.
51. Yang Z, Wang T, Dejun Wu, et al. RNA N6-methyladenosine reader IGF2BP3 regulates cell cycle and angiogenesis in colon cancer. *J Exp Clin Cancer Res.* 2020;39:203. <https://doi.org/10.1186/s13046-020-01714-8>.
52. Wang Y, Jia-Huan Lu, Qi-Nian Wu, et al. lncRNA LINRIS stabilizes IGF2BP2 and promotes the aerobic glycolysis in colorectal cancer. *Mol Cancer.* 2019;18: 174. <https://doi.org/10.1186/s12943-019-1105-0>.
53. Lou X, Ning J, Liu W, et al. YTHDF1 Promotes Cyclin B1 Translation through m 6 A modulation and contributes to the poor prognosis of lung adenocarcinoma with KRAS/TP53 co-mutation. *Cells.* 2021;10:1669. <https://doi.org/10.3390/cells10071669>.
54. Gao Y, Ouyang X, Zuo Li, et al. R-2HG downregulates ERα to inhibit cholangiocarcinoma via the FTO/m6A-methylated ERα/miR16-5p/YAP1 signal

- pathway. *Mol Ther Oncolytics*. 2021;23:65–81. <https://doi.org/10.1016/j.omto.2021.06.017>.
55. Pan J, Xu L, Pan H. Development and Validation of an m6A RNA methylation regulator-based signature for prognostic prediction in cervical squamous cell carcinoma. *Front Oncol*. 2020;10:1444.
  56. Cho S, Lee G, Pickering BF, Jang C, Park JH, He L, Mathur L, Kim SS, Jung S, Tang HW, et al. mTORC1 promotes cell growth via m(6)A-dependent mRNA degradation. *Mol Cell*. 2021;81:2064–2075.e2068.
  57. Villa E, Sahu U, O'Hara BP, Ali ES, Helmin KA, Asara JM, Gao P, Singer BD, Ben-Sahra I. mTORC1 stimulates cell growth through SAM synthesis and m(6)A mRNA-dependent control of protein synthesis. *Mol Cell*. 2021;81:2076–2093.e2079.
  58. Zhao Q, Zhao Y, Hu W, Zhang Y, Wu X, Lu J, Li M, Li W, Wu W, Wang J, et al. m(6)A RNA modification modulates PI3K/Akt/mTOR signal pathway in gastrointestinal cancer. *Theranostics*. 2020;10:9528–43.
  59. Liu J, Eckert MA, Harada BT, Liu SM, Lu Z, Yu K, Tienda SM, Chryplewicz A, Zhu AC, Yang Y, et al. m(6)A mRNA methylation regulates AKT activity to promote the proliferation and tumorigenicity of endometrial cancer. *Nat Cell Biol*. 2018;20:1074–83.
  60. Lan N, Lu Y, Zhang Y, Pu S, Xi H, Nie X, Liu J, Yuan W. FTO—a common genetic basis for obesity and cancer. *Front Genet*. 2020;11: 559138.
  61. Chen H, Gao S, Liu W, Wong CC, Wu J, Wu J, Liu D, Gou H, Kang W, Zhai J, et al. RNA N(6)-Methyladenosine methyltransferase METTL3 facilitates colorectal cancer by activating the m(6)A-GLUT1-mTORC1 axis and is a therapeutic target. *Gastroenterology*. 2021;160:1284–1300.e1216.
  62. Wang F, Liao Y, Zhang M, Zhu Y, Wang W, Cai H, Liang J, Song F, Hou C, Huang S, et al. N6-methyladenosine demethyltransferase FTO-mediated autophagy in malignant development of oral squamous cell carcinoma. *Oncogene*. 2021;40:3885–98.
  63. Sun Y, Li S, Yu W, Zhao Z, Gao J, Chen C, Wei M, Liu T, Li L, Liu L. N(6)-methyladenosine-dependent pri-miR-17-92 maturation suppresses PTEN/TMEM127 and promotes sensitivity to everolimus in gastric cancer. *Cell Death Dis*. 2020;11:836.

### Publisher's Note

Springer Nature remains neutral with regard to jurisdictional claims in published maps and institutional affiliations.

Ready to submit your research? Choose BMC and benefit from:

- fast, convenient online submission
- thorough peer review by experienced researchers in your field
- rapid publication on acceptance
- support for research data, including large and complex data types
- gold Open Access which fosters wider collaboration and increased citations
- maximum visibility for your research: over 100M website views per year

At BMC, research is always in progress.

Learn more [biomedcentral.com/submissions](https://biomedcentral.com/submissions)

